Immunology & Cell Biology 2025; **103**: 45–59
www.wileyonlinelibrary.com/journal/icb

ORIGINAL ARTICLE

OPEN

Characterization of cellular and molecular immune components of the painted white sea urchin *Lytechinus pictus* in response to bacterial infection

Katherine T Nesbit[1,a], Alexis Cody Hargadon[2,a], Gloria D Renaudin[2], Nicholas D Kraieski[3], Katherine M Buckley[3], Emily Darin[1], Yoon Lee[2], Amro Hamdoun[2] & Catherine S Schrankel[1]

1 Department of Biology, San Diego State University, San Diego, CA, USA
2 Scripps Institution of Oceanography, University of California San Diego, San Diego, CA, USA
3 Department of Biological Sciences, Auburn University, Auburn, AL, USA

Keywords
Bacterial infection, innate immunity, sea urchin, SRCR, stem cell

Correspondence
Catherine S Schrankel, Department of Biology, San Diego State University, 5500 Campanile Dr., San Diego 92182, CA, USA.
E-mail: cschrankel@sdsu.edu

[a]Co-first authors.

Received 8 January 2024;
Revised 7 June, 17 July and 30 September 2024;
Accepted 1 October 2024

doi: 10.1111/imcb.12828

Immunology & Cell Biology 2025; **103**: 45–59

Abstract

Sea urchins are basal deuterostomes that share key molecular components of innate immunity with vertebrates. They are a powerful model for the study of innate immune system evolution and function, especially during early development. Here we characterize the morphology and associated molecular markers of larval immune cell types in a newly developed model sea urchin, *Lytechinus pictus*. We then challenge larvae through infection with an established pathogenic *Vibrio* and characterize phenotypic and molecular responses. We contrast these to the previously described immune responses of the purple sea urchin *Strongylocentrotus purpuratus*. The results revealed shared cellular morphologies and homologs of known pigment cell immunocyte markers (*PKS*, *srcr142*) but a striking absence of subsets of perforin-like *macpf* genes in blastocoelar cell immunocytes. We also identified novel patterning of cells expressing a scavenger receptor cysteine rich (SRCR) gene in the coelomic pouches of the larva (the embryonic stem cell niche). The SRCR signal becomes further enriched in both pouches in response to bacterial infection. Collectively, these results provide a foundation for the study of immune responses in *L. pictus*. The characterization of the larval immune system of this rapidly developing and genetically enabled sea urchin species will facilitate more sophisticated studies of innate immunity and the crosstalk between the immune system and development.

INTRODUCTION

The immune system continuously receives inputs from pathogenic, benign and beneficial microbes.[1,2] To understand how different microbial inputs impact immunity, a breadth of robust experimental systems is needed. One example is the sea urchin, which begins life with free-swimming embryonic and larval stages that develop as "orphans" in a microbially rich marine environment. Mature larvae subsequently undergo metamorphosis in response to a variety of microbial cues to transition into an adult body plan and settle in a benthic environment. Many facets of the innate immune system are critical for survival in the marine environment.

Echinoderm embryos have long been used to identify cellular responses to non-self, from foreign objects[3,4] to potential pathogens,[5] especially those naturally present in their ocean environments.[6–9] Prior work on echinoderm innate immunity has largely been undertaken in the historic model, the purple sea urchin, *Strongylocentrotus purpuratus*.[7,8,10,11] In purple sea urchins, the cellular immune components are made from a mixed population of cells, with five key cell types identified in adults and

early larvae.[8] The most notable larval cell type among these is the pigment cell. Pigment cells contain an autofluorescent naphthoquinone called echinochrome A, which is encapsulated in granules and exhibits antimicrobial properties.[12] During development, pigment cells arise from a population of non-skeletal mesodermal (NSM) cells at the aboral vegetal pole.[8,13] Meanwhile, the remaining four immune cell types, collectively termed blastocoelar cells, arise from the oral side of the vegetal pole during development.[14]

Several important molecular components of the innate immune system have been characterized in the purple sea urchin genome.[7,8,14] These include key gene families encoding pattern recognition receptors and signaling factors (e.g. Toll-like receptors, scavenger receptor cysteine-rich [SRCR] genes and NFkB pathway homologs), the complement system (e.g. C3 and thioester-containing proteins), as well as effector genes (e.g. macpf containing perforin-like members) and well-known cytokines and growth factors (e.g. interleukins, tumor necrosis factor genes and macrophage inhibitory factors).[15] During early larval infection, the cellular and molecular components of the immune system are activated and respond in a coordinated, dose-dependent and reversible fashion.[8] Pigment cells interact with other immune cells and migrate towards sites of gut infection. These organism-wide responses are driven by dynamic gene expression levels throughout the infection period.[8]

One current limitation in the field is that immune research in the purple sea urchin is restricted by the relatively slow development of this species, making perturbations time-consuming and labor-intensive. Furthermore, stable genetic modifications of purple urchins are not practical due to their long generation times of 1 to 2 years. The painted white urchin, *Lytechinus pictus,* is a fast-developing, genetically enabled species that facilitates easier access to later life-history stages.[16–18] With large, optically transparent larvae, smaller adult body sizes, and a host of tools available for manipulating and generating animal lines, this species is well-poised to resolve many of the limitations previously encountered in other sea urchin model species.

To lay the groundwork for the study of the immune system in this species, we sought to characterize cellular and molecular components of the *L. pictus* innate immune system, drawing important comparisons to the well-established, related purple sea urchin, *S. purpuratus*. Here we also describe the response of the larva to bacterial infection and identify a new territory of immune gene expression in the coelomic pouches, the embryonic stem cell niche. We propose future work to investigate how the immune system may be involved in developmental transitions such as metamorphosis. This foundation will also grow our understanding of how combinatorial exposures from the environment may influence the function of the immune system across several life stages.

RESULTS

Cellular components of the *L. pictus* immune system include morphologically distinct pigment and blastocoelar subtypes

Previous characterizations of echinoderm larval immune systems used microscopy to identify cell types with immune characteristics, such as phagocytic and migratory behaviors.[4,5,8] We took a similar approach with time-lapse DIC imaging to identify cell subtypes in *L. pictus*. The *L. pictus* larval immune system is composed of a heterogeneous group of cells that are readily identifiable by 3 days post-fertilization (dpf) (Figure 1a), based on distinct morphologies first categorized by Ho *et al.* (2016).[8] This is earlier than in *S. purpuratus*, which takes between 5 and 7 days to reach a comparable developmental stage in which all immunocytes are morphologically distinct and terminally differentiated. The most conspicuous cell type involved in the larval sea urchin immune response are the pigment cells (PCs) which are normally embedded in the ectoderm of the animal in stellate morphologies (Figure 1b).

Other immune cell types identified in the larva include globular cells (Figure 1c), filopodial cells (Figure 1d), ameboid cells (Figure 1e) and ovoid cells (Figure 1f), which are identifiable by their morphological features, and rapid motility in the case of ameboid cells (Supplementary videos 1–4). The globular cells have a relatively large size and irregular shape (Figure 1c). In contrast, a characteristic feature of filopodial cells are long narrow projections from the main cell body (Figure 1d, black arrow). These extensions likely play important roles in sensing, are highly labile, and help to form a dynamic syncytium within the body cavity of the larva. The ovoid cells are identifiable by a circular "dimple" (Figure 1f) on the body of the cell. There are very few of these motile cells in the animal, and in *L. pictus* we only observed ovoid cells in larvae exposed to *Vibrio diazotrophicus*.

Homologs of immunocyte molecular markers are expressed in the *L. pictus* immune system

In addition to identifying the cellular components of the innate immune system of *L. pictus*, a subset of

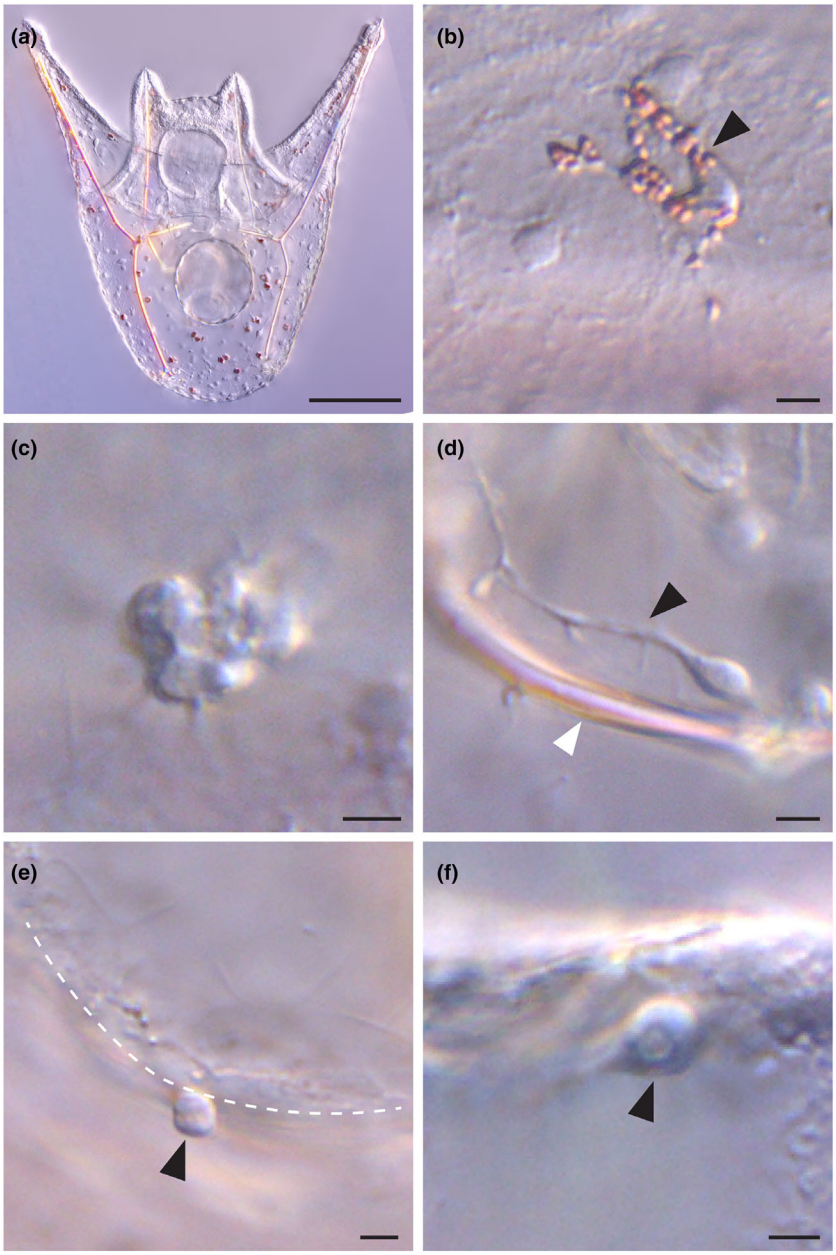

Figure 1. Larval immune cell types in the sea urchin *Lytechinus pictus*. **(a)** Larva at 3 days post-fertilization (dpf). **(b)** Stellate pigment cell (black arrow, non-active morphology). **(c)** Globular cell. **(d)** Filopodial cell. Black arrow denotes the long filopodia extending from the cell body. White arrow indicates a skeletal rod of the larva. **(e)** Ameboid cell (black arrow). White dashed line outlines the epithelia of the gut. The "tail" of these typically comma-shaped cells is out of view. **(f)** Ovoid cell (black arrow) imaged from a larva infected with *Vibrio diazotrophicus* for 28 h. Scale for **a** = 100 μm. Scale for all other panels = 5 μm.

characteristic molecular markers for immune cell types were localized in 3-day-old, uninfected larvae using a novel high-throughput application of HCR-RNA FISH[19–21] (probe sets for molecular targets in *L. pictus* are provided in Supplementary table 1 and negative hairpin controls are shown in Supplementary figure 1).

We identified homologs for immune markers in the genome of *L. pictus*[18] with roles in pattern recognition, effector response and cytokine signaling, which are important molecular markers of immunocytes in the related purple urchin (e.g. *PKS*, *srcr142*, *macpf* and *IL17*).[8]

PKS, which encodes a polyketide synthase, localized as expected to the pigment cells of the larva. The signal was evenly distributed throughout pigment cells in the larval ectoderm and was consistent across all larvae at the 3 dpf feeding stage (Figure 2a). The *L. pictus* homolog of *srcr142* also localized to pigment cells in the ectoderm (Figure 2b). Surprisingly, we also observed localization of *srcr142* transcripts in coelomic pouches in ~82% of larvae – primarily in the left pouch (Figure 2b′–b″, Supplementary table 3; $n = 60/75$). However, some variation in the patterning in the coelomic pouches is evident. In ~8% of the larvae scored, cells in the right pouch expressed *srcr142* in addition to those in the left pouch (Figure 2c, Supplementary table 3; $n = 6/75$). Some larvae (~9%, $n = 7/75$) had no expression in either coelomic pouch. This is a unique feature as there is no previous documentation of *srcr142* expression in the coelomic pouches of *S. purpuratus*.

Another interesting difference in the molecular immune repertoire of *L. pictus* is in the expression of a *L. pictus* perforin-like factor containing the Membrane Attack Complex/PerForin (macpf) domain. In mammals, perforins help to damage bacteria or infected host cells by using the macpf domain to create pores in cell membranes. The purple sea urchin larva expresses *macpfA2* in globular cells.[8] However, we could not find a direct homolog to *macpfA2* in *L. pictus* (nor were we able to identify one in the close relative *L. variegatus*). Instead, a different macpf-domain containing transcript, *macpfE2*, was identified and localized (Supplementary figure 2, Supplementary table 2). The *L. pictus macpfE2* is expressed in a distinct ring of cells that encircle the apical portion of the midgut (stomach) (Figure 2d–f), much like the localization pattern for the *S. purpuratus macpfE*.[22] Variation in patterning is again evident with this molecular target, and we observed varying levels of baseline expression between mate pairs. Some genetic backgrounds displayed a distinct complete ring in the majority of larva (Figure 2f, Supplementary table 4), while others had a comparatively lower number of *macpfE2*-positive cells encircling the gut that formed semi-circular patterns (Figure 2e), or partial segments (Figure 2d) around the circumference of the stomach. These results are consistent with the gene expression profiles of acinar, exocrine-like cells that encircle the anterior portion of the stomach.[23–25] Overall, the identification and localization of molecular markers of immunity in immune-quiescent 3 dpf larvae reveal similar patterning to the purple sea urchin, with unique differences in the territories occupied by *srcr142*-positive cells, and greater degrees of variation in expression for *macpfE2*-positive cells, along with the absence of any *macpfA* homologs.

Pigment cells migrate to the gut in response to vibrio infection

Pigment cells, in coordination with the other immune cell types, are known to function against larval infection in a microbially rich environment.[8] To assess whether pigment cells of *L. pictus* responded to infection similarly, we exposed larvae to the marine nitrogen-fixing bacterium *V. diazotrophicus*. This species is the pathogen previously used in the purple sea urchin infection model,[8] and was first isolated from the gut of the sea urchin.[26] Upon infection with *V. diazotrophicus*, the pigment cells dissociate from the ectoderm and migrate through the blastocoel towards the gut, with more pigment cells migrating as infection progresses (Figure 3a), compared with uninfected controls. Migrating cells have a more rounded morphology, different from un-activated cells, which are more stellate, and cluster around the gut (Figure 3b, c). The pigment cell migration is accompanied by inflammation of the gut epithelium and constriction of the gut lumen (Figure 3b, c for T_0 and T_{24} h post exposure [hpe], respectively). Although there is individual variation in the intensity of the response (Figure 3a), the infected larvae have a greater number of activated, migrating cells than their uninfected counterparts.

We did not observe noticeably different pigment cell migration phenotypes at earlier points in infection, e.g. by 2 hpe (Supplementary figure 3), despite the more rapid development of *L. pictus*. Thus, it appears that the dynamics responsible for the cellular coordination during immune responses may be under similar temporal control to the *S. purpuratus* infection model, despite the different developmental timelines for differentiation of these cell types in these two sea urchin species. Overall, the *L. pictus* phenotype of pigment cell migration in response to challenge with *V. diazotrophicus* infection recapitulates the response to infection that is observed in the *S. purpuratus* infection model, making *L. pictus* an excellent candidate for comparative immunology studies.

Immune cell markers exhibit conserved and divergent domains of expression post-vibrio infection

To better understand the variation in immune gene patterning during immune challenge, we applied our HCR-RNA FISH pipeline[27] to larvae that had been exposed to *V. diazotrophicus*. We assessed localization from 0 to 24 hpe (Figures 4 and 5). Sibling larvae that did not receive *Vibrio* exposure ("unexposed") were collected at each time point as a control (Supplementary figures 4 and 5).

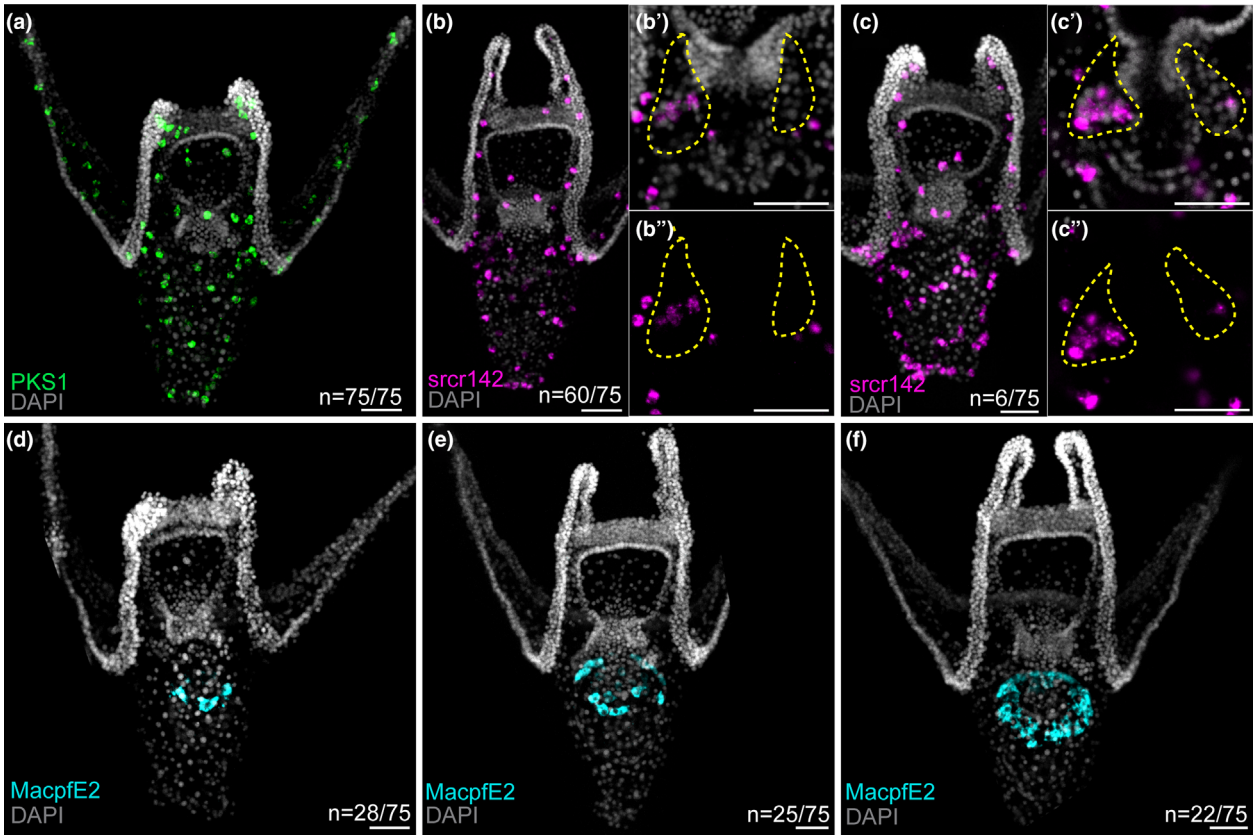

Figure 2. Basal expression of molecular markers of immune cells in *Lytechinus pictus* larvae. **(a)** *PKS1* is localized in pigment cells of the larvae. Signal is evenly distributed in pigment cells embedded in the ectoderm of the animal. **(b, c)** Localization of *srcr142* transcript in the larvae occurs in pigment cells as well as in coelomic pouches of the larva, with variability in the number of *srcr142*-positive cells observed in the right pouch (**b′–b″** and **c′–c″**, with and without DAPI overlay). All lower magnification images **(b, c)** are maximum intensity projections from Z-stacks of whole fixed larvae at 3 dpf. Insets **(b′–b″)** and **(c′–c″)** show individual slices from the Z-stacks from the same larvae shown in **(b)** and **(c)** respectively, at higher magnification. Coelomic pouches are outlined with yellow dashed lines. **(d–f)** Expression of *macpfE2* in the gut is variable, but all *macpfE2*-positive cells localize to a ring, or parts of a ring around the stomach. Some larvae have lower numbers of expressing cells **(d)**, while others have enough positive cells to completely encircle the gut **(f)**. Quantification of each type of gene pattern scored is listed above the scale bar (n = 75 larvae combined from three distinct mate pairs). Genes labeled are noted in the lower left of each panel (DAPI – gray, *PKS1* – green, *srcr142* – magenta and *macpfE2* – cyan). Scale = 25 μm for all panels and insets. Detailed quantification of phenotypes is available in Supplementary tables 3 and 4.

The number of *srcr142*-positive cells in the coelomic pouches of bacteria-exposed larvae increased over the 24-h exposure period, as early as 6 hpe but with the most notable change at later stages of infection (e.g. 12–24 h; Figures 4a–d and 5a). Quantitative fluorescence measurements also supported this observation and revealed significant differences in the fluorescence intensity of the *srcr142* signal in the coelomic pouches between T_0 uninfected larvae and T_{24} *Vibrio*-exposed larvae (Figure 6a; $P = 0.0059$). We hypothesize that this observation is not a proliferative response due to the birth of new cells, because the intensity of nuclear DAPI signal is not significantly different between treatments (Figure 6b). Furthermore, we did not observe live pigment cells localizing to the coelomic pouches in larvae after 24 h of infection (Figure 3c). 3D rendering of *srcr142*-positive cells in *Vibrio*-exposed larvae (Figure 7) confirmed the expansion of coelomic pouch expression territories throughout the course of infection, with a modest increase in the left and a more pronounced increase of *srcr142* signals in the right pouch. It is possible that the observed increase in signal represents novel *de novo* expression of *srcr142* that is initiated in coelomic pouch cells in response to bacterial exposure. The hypothesis of newly activated expression will be the subject of future investigation.

In addition to the novel coelomic pouch patterning, in *Vibrio*-exposed larvae, *srcr142* localization was found

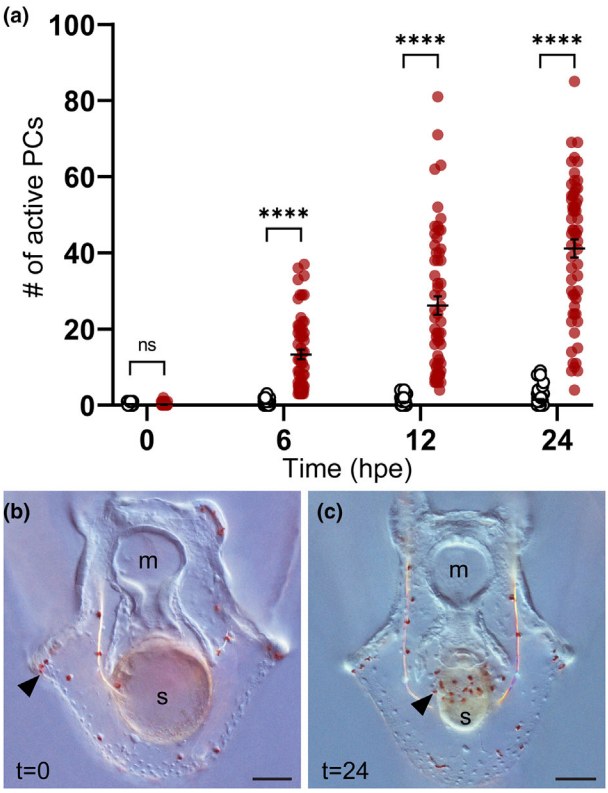

Figure 3. Infection with *Vibrio diazotrophicus* causes significant differences in pigment cell activation and migration to the gut. **(a)** Quantification of the migratory pigment cell phenotype pooled from six genetically distinct mate pairs. White circles are control larvae that have not been exposed to *Vibrio*, red circles are sibling larvae that have been exposed to *Vibrio*. Statistical labeling: ns, not significant ($P > 0.05$); ****$P < 0.0001$. **(b, c)** Representative micrographs of the phenotypic response to *V. diazotrophicus* exposure. Uninfected larvae at 3 dpf **(b)** have little to no activated pigment cells, and instead these cells are localized to the ectoderm (black arrow). The stomach "s" is large with a thin epithelium, and the mouth "m" is annotated. At 24 h post-exposure (hpe) to *Vibrio*, the larval stomach (S) has become inflamed and constricted, and pigment cells (black arrow) are clustering at the stomach **(c)**.

evenly dispersed in pigment cells scattered throughout the ectoderm and blastocoel. We also observed localization in pigment cells that had congregated at the gut by 24 h post-exposure in some larvae (Figure 4d). Although there is colocalization of *srcr142* and *PKS* in some pigment cells of the larva (Supplementary figure 5), the pigment cells are known to be a heterogenous population.[8] In line with this, we observed strong differences in the target territories of *srcr142*-positive cells and *PKS*-positive cells: *srcr142*-positive cells occurred primarily at the coelomic pouches, and *PKS*-positive cells were observed primarily surrounding the gut by 24 hpe (Figure 5a, b, Supplementary figure 5). This does not rule out the occurrence of *PKS*-positive cells in the coelomic pouches, and indeed we did observe a small number of larvae with one to two *PKS*-positive cells in the coelomic pouch (Supplementary figure 6, Supplementary videos 7 and 8. However, the overall trends in localization post-*Vibrio* exposure differ for these two immune cell markers, suggesting that subpopulations of pigment cells or coelomic pouch cells play specific roles with distinct responses to bacterial infection. To our knowledge, *srcr142* has not been observed in the coelomic pouches of *S. purpuratus*, so these observations in *L. pictus* provide a potentially novel cellular and molecular response during infection.

In contrast, the control sibling larvae that were not challenged with *Vibrio* only exhibited modest variations in *srcr142* localization over a 24-h period. Comparable to previous immunoquiescent mate pairs observed (Figure 2), transcripts of the scavenger receptor (*srcr142*) at T_0 are detected scattered in the larval ectoderm and primarily in the left coelomic pouch, with a small subset of larvae exhibiting faint expression in the right pouch as well (Figure 4a). We observed this pattern in roughly half of the unexposed larvae (Figure 5a, Supplementary table 3).

In summary, we observed stronger patterning of srcr142 in the coelomic pouches of *Vibrio*-exposed larvae. However, the intensity of the response does vary within and among mate pairs, as quantified by the number of *srcr142*-positive cells that localized to distinct territories including the coelomic pouches (Supplementary table 3). This is unsurprising given the known variation of pigment cell marker gene expression and scavenger receptor gene expression[28] between individuals, which again may collectively reflect the subtypes of pigment cells distinguishable only at the molecular level.[8]

The patterning of the stereotypical pigment cell marker *PKS1* was also examined. As reflected in the phenotypic quantification of pigment cell migration (Figure 3a), we saw variability in the number of *PKS1*-positive cells that migrated to the gut throughout infection. Overall, *PKS*-positive cells migrated from locations in the ectoderm to aggregate at the gut (Figure 4e–h). While most *PKS1*-positive pigment cells were observed to round and migrate to the gut, there was a distinct variation in the rate and magnitude of response between mate pairs (Figure 5b, Supplementary table 4). After 6 h of exposure to *V. diazotrophicus*, pigment cells are present throughout the ectoderm in most larvae, while only larvae from one of the three mate pairs showed a stronger localization to the gut (Supplementary table 4). Migration was most distinct in this mate pair at 12 and 24 h of exposure, where a larger proportion of larvae showed most of the

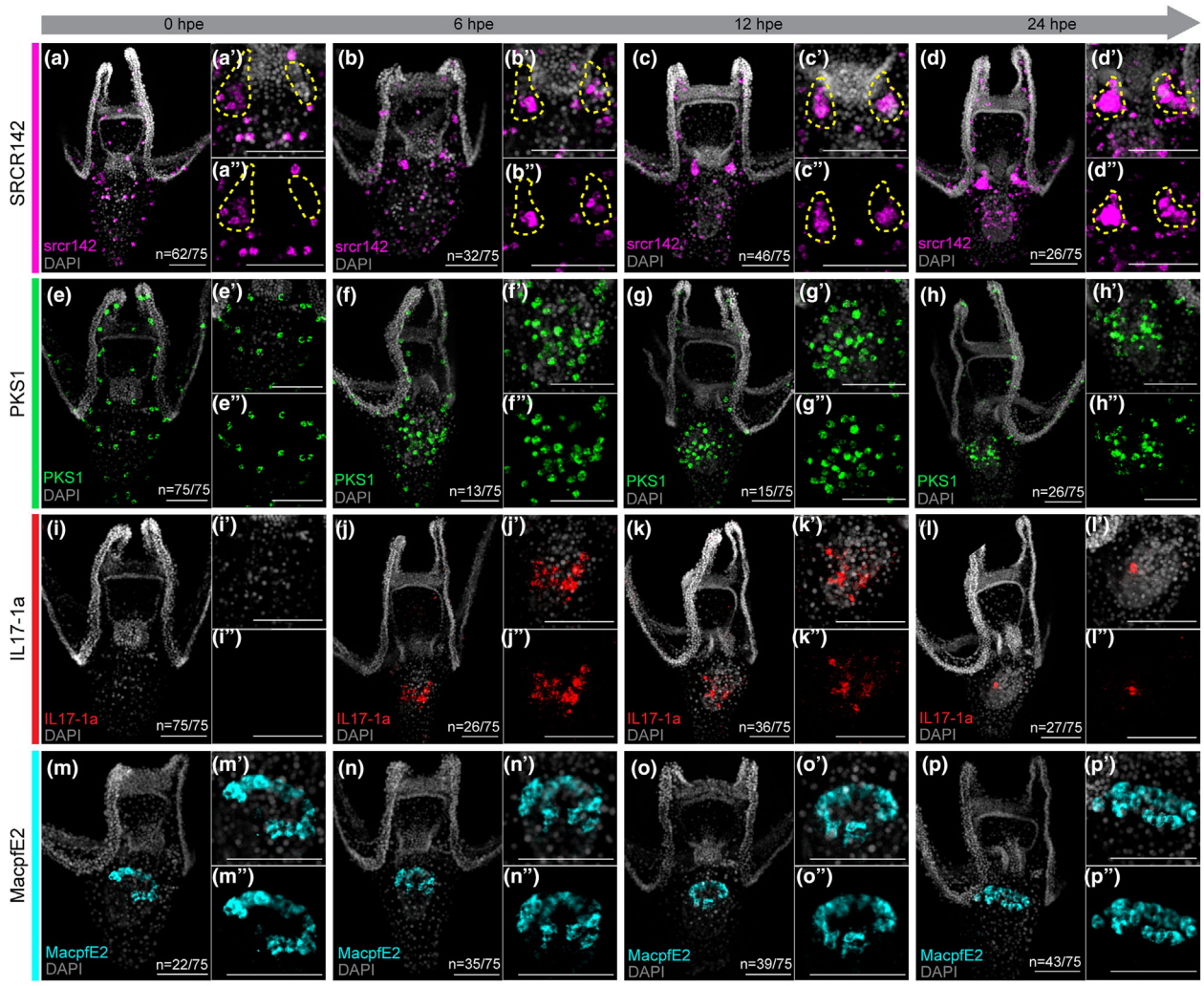

Figure 4. Immune gene markers respond variably to *Vibrio diazotrophicus* infection. **(a)** *srcr142* transcripts are localized to pigment cells throughout the larval body and within cells of the left and right coelomic pouch. **(b–d)** *srcr142* transcripts are evident in several cells in the left CP as well as within 1–2 cells in the right pouch at 6 h post-exposure (hpe; **b–b″**), increasing in the number of cells in both coelomic pouches through 24 hpe **(c–d″)**. Boxed insets highlight the localization of *srcr142*-positive cells within the coelomic pouches (outlined in yellow dashed lines), both with DAPI overlay **(a′–d′)** and without **(a″–d″)**. **(e–h) (e)** Prior to bacterial exposure, pigment cells marked by *PKS1* are evenly distributed throughout the ectoderm; **(f)** cells begin to round and migrate towards and surround the midgut by 6 hpe; **(g)** tightly surrounding the midgut at 12 hpe; and **(h)** beginning to migrate away at 24 hpe. The box insets highlight the localization of pigment cells around the midgut within each figure, both with DAPI overlay **(e′–h′)** and without **(e″–h″)**. **(i–l)**. **(i)** *IL17-1a* transcription is absent in larvae prior to exposure; **(j, k)** At 6 and 12 hpe, transcription of *IL17-1a* is localized to the midgut, with a slight decrease in abundance at hour 12; **(l)** By 24 hpe, transcription of *IL17-1a* is generally present in about 1–3 cells near the midgut. The box insets highlight the localization of *IL17-1a*-positive cells near the midgut within each figure, both with DAPI overlay **(i′–l′)** and without **(i″–l″)**. **(m–p)** *MacpfE2* transcription is localized to cells surrounding the apical portion of the midgut. Little variation is observed throughout exposure **(n–p)**; however, the number of cells transcribing *macpfE2* varies between mate pairs (see Supplementary table 4). The box insets highlight the localization of *macpfE2*-positive cells in the midgut within each figure, both with DAPI overlay **(m′–p′)** and without **(m″–p″)**. Quantification of the phenotype is shown in the lower right of each panel (*n* = # of larvae out of the total scored from three mate pairs). Scale for all panels = 50 μm.

pigment cells enveloping the gut epithelium. The other two mate pairs showed a much slower response and were only seen to initiate pigment cell migration by hour 24 (Supplementary table 4). Sibling larvae that were not exposed to *Vibrio* showed no change in ectodermal localization of PKS^{+} cells throughout the 24-h period (Figure 5b, Supplementary figure 4).

Beyond pigment cell markers, we were interested in the patterning dynamics of known signaling cytokines (*IL17*) and potential effectors (*macpfE2*) in the gut. During gut

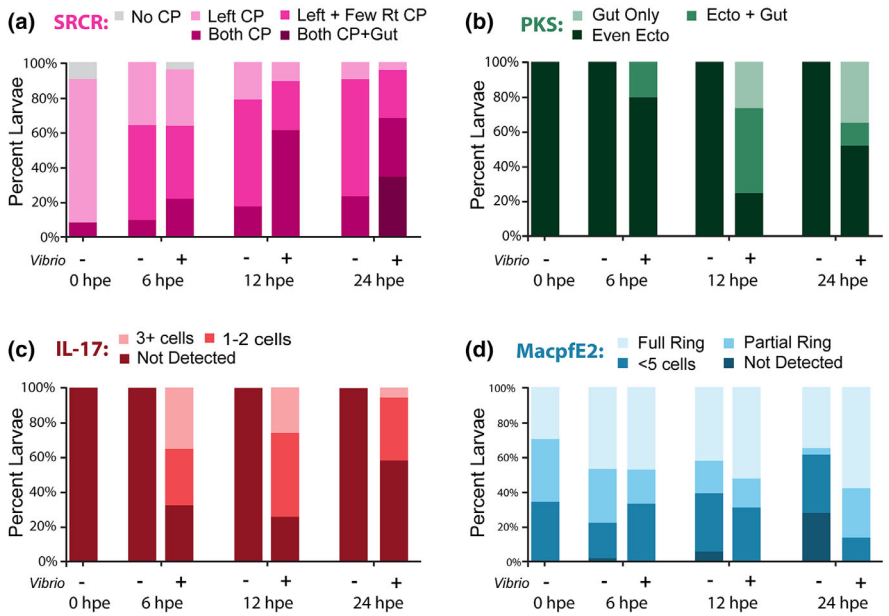

Figure 5. Quantification of immune gene expression territories in response to bacterial exposure. **(a)** Patterning of *srcr142*; **(b)** *PKS*; **(c)** *IL17-1a*; and **(d)** *macpfE*. Scoring for all genes is pooled from 25 larvae each from three mate pairs (n = 75 total). Above each stacked bar, "−" indicates control, unexposed larvae and "+" indicates larvae exposed to *Vibrio diazotrophicus*. Larvae were assessed at 0, 6, 12 or 24 h post-exposure (hpe).

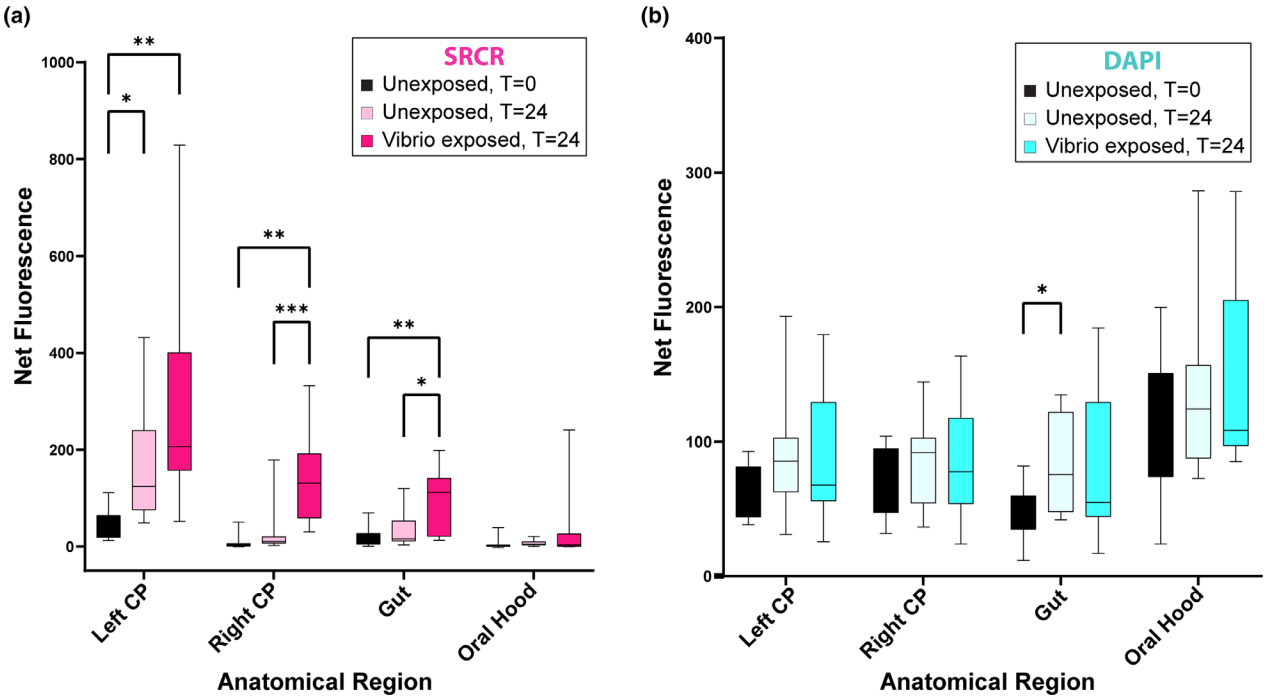

Figure 6. The intensity of srcr142 signal increases in the coelomic pouches during bacterial exposure. **(a)** Distribution of net fluorescence intensity of *srcr142* signal. Control larvae without exposure to bacteria at T_0 (black), control larvae at T_{24} (light pink), and larvae exposed to *Vibrio* at T_{24} (magenta). **(b)** Distribution of DAPI signal of control larvae without exposure to bacteria at T_0 (black), control larvae at T_{24} (light blue) and larvae exposed to *Vibrio* at T_{24} (cyan). Measurements are pooled from five larvae each from three mate pairs (n = 15 total). Asterisks denote statistical significance for comparisons between treatments within an anatomical region as determined by two-way ANOVA. Comparisons that are not significantly different are not marked. *$P < 0.03$; **$0.0021 < P < 0.03$; *** = 0.0059.

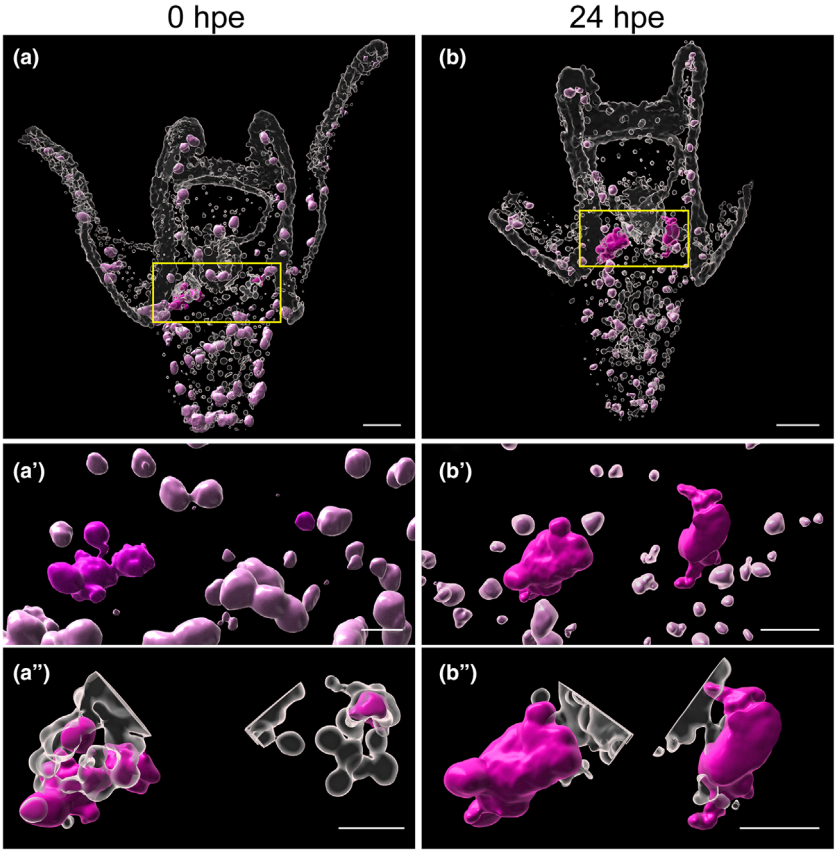

Figure 7. Three-dimensional rendering of srcr142 expression in the coelomic pouches of bacteria-exposed larvae. **(a, a″)** Representative larva at T_0, with DAPI displayed in white with transparency. Cells that are *srcr142*-positive are filled with light pink, and cells that are *srcr142*-positive and located at the coelomic pouch are filled in with magenta. Yellow box indicates the region for coelomic pouch-centered insets showing only *srcr142*-positive cells (DAPI removed; **a′**) or coelomic pouches rendered with *srcr142*-positive cells in magenta and DAPI in white with transparency **(a″)**. **(b, b″)** Representative larva at T_{24} of *Vibrio* exposure. Color and inset schemes are the same as in Panel A. Scale for panel **(a)** and **(b)** = 100 μm. Scale for **a′, a″** and **b′, b″** = 50 μm. Additional views of the 3D renderings are provided in Supplementary videos 5 and 6.

infection and inflammation in mammals and *S. purpuratus*, interleukin 17 (IL17) genes are upregulated in epithelial cells, where they are required for activating downstream immune responses.[7] To see whether this response is conserved in *L. pictus* we first identified the *IL17* gene family in the genome (Supplementary figure 7, Supplementary tables 5–7). We found that like other sea urchins, *L. pictus* has 11 subfamilies of *IL17* genes, including the Group 1 paralog that is primarily activated in the *S. purpuratus* larval gut post-*Vibrio* infection (*IL17-1a*).[7] *LpIL17-1a* transcripts were not observed in unexposed larvae (Figures 4i and 5c; Supplementary figure 4i–l, Supplementary table 4). However, the activation of this conserved cytokine is relatively swift, and by 6 h post-exposure there is strong signal detected within the gut of some animals (Figure 4j). The signal decreases slightly by 12 h (Figure 4k). After 24 h of bacterial exposure, the majority of larvae expressed *IL17-1a* in an average of only 1–2 cells on the gut epithelium, signifying attenuation of the *IL-17* expression (Figure 5c). Our HCR RNA-FISH localizations are similar to those observed in *S. purpuratus* during bacterial challenge.[7,8]

We next looked at the patterning response of the potential effector gene *macpfE2*,[8,29] which to our knowledge has not been localized during exposure to bacteria in other urchin species. Transcripts were localized to a clear ring of cells that encircled the larval stomach. This pattern remained stable throughout the course of a 24 h infection with *V. diazotrophicus*. Interestingly, in larvae that were not exposed to *Vibrio* we observed an overall decline in the number of *macpfE2*-positive cells over the experimental period between 3 and 4 dpf in two of the three mate pairs scored (Figure 5d, Supplementary table 4). By the 24-h time point (equivalent to 4 days post-fertilization), two

of the three control sibling mate pairs exhibited a fluorescent signal in only 1–3 cells in some larvae, but it was completely absent in most larvae (Figure 5d, Supplementary figure 4m–p). Only one of the three control mate pairs did not exhibit a decline in macpfE2-positive cells over the experimental period. Notably, all control larvae were not fed during the 24 h exposure experiment. We hypothesize that endogenous expression of *macpfE2* in the gut may require active feeding to take place to be sustained, but this remains to be tested in future investigations.

In summary, the data presented here provide an initial characterization of the cellular and molecular components of the *L. pictus* immune system. This first look at *L. pictus* immunity reveals important similarities to existing echinoderm models, as well as novel features that generate exciting new research directions.

DISCUSSION

Echinoderms have long been an important whole-animal model system that has provided valuable contributions to our understanding of the origins and function of innate immunity.[3,9,30] The sea urchin larva provides a streamlined *in vivo* context for immune interactions without the limitations imposed by single-cell systems or the complexities that arise with adaptive immune responses.[31] The data presented here provide a foundation for broader examination of innate immunity, especially within comparative contexts spanning developmental and evolutionary time scales. Characterizing the similarities and differences between the *L. pictus* immune system and other echinoderms (and invertebrates overall) could inform our understanding of the origins for innate immune machinery, which often serve as the evolutionary precursors to adaptive components.[9,15,31]

The *L. pictus* immune system shares many similar features with, and exhibits important differences from, the well-characterized immune system of the related purple sea urchin. For example, *L. pictus* shares five key immune cell morphologies (Figure 1) with *S. purpuratus*, including the conspicuous pigment cells that migrate throughout the larval body and congregate at sites of infection when the immune system is activated. We found known pigment cell markers (*PKS* and *srcr*) present in *L. pictus* pigment cells, and these cells migrated towards inflamed tissues. Another similarity to infected *S. purpuratus* larvae that we observed in *L. pictus* was the activation of *IL17* cytokines in response to bacterial infection. Thus, although the number of *IL17* genes differs within these two Echinoderm species (29 total genes in *S. purpuratus* compared with 16 genes in *L. pictus*; Supplementary figure 7), the gut-specific activation of IL17 homologs remains conserved.

In contrast, when we examined other molecular markers of immunocytes, we found clear differences between these species. Although *L. pictus* and *S. purpuratus* genomes encode several Membrane Attack Complex/PerForin gene families, the *macpfA* subgroup appears to be absent in urchin species from the genus *Lytechinus* (Supplementary figure 2). Although the function of *macpfA2* in *S. purpuratus* globular cells is not yet known, this highlights the importance of careful annotation of these gene families. This is especially important for rapidly evolving genes[6,10] or when comparing immune components across evolutionary time scales. The purple sea urchin is approximately 40 million years diverged from *L. pictus*[32–34] and thus differences in molecular features are expected despite the overall striking congruence of cellular morphologies and phenotypes across urchin species.

Another difference in the molecular markers of immunity investigated in this study is the patterning of *srcr142*-positive cells in the coelomic pouches of the larva preceding bacterial exposure (Figure 2, Supplementary Table 3) and the expansion of this expression territory throughout the course of infection (Figures 4, 5a, 6 and 7, Supplementary Table 4). Localization of this particular srcr gene has not been previously reported in the coelomic pouches. Thus, our data represent a novel finding that warrants future investigation on the function of this immune marker in the coelomic pouches, before and during immune challenges.

Coelomic pouches house both stem cells and the primordial germ cells (PGCs) of the larva, which are progenitors for eventual egg or sperm of the metamorphosed adult. It is possible that the PGCs are protected by a population of immune-responsive cells that increases in activity during infection with bacteria. The ability for bacterial infection to impede fertility, destroy germ cells, or disrupt differentiated egg and sperm cells is documented in humans and other mammals with adaptive immune responses.[35–37] Damage to DNA in germ cells is also linked with induction of innate immune responses, for example in *Caenorhabditis elegans*.[38] Our finding of a high density of cells with expression of immune markers in the coelomic pouch in *L. pictus* may hint at similar reproductive vulnerabilities during infection and a corresponding basal protective mechanism in an organism that lacks adaptive immune cell types. Alternatively, *de novo* post-exposure *srcr142* expression in the coelomic pouches may represent the development of new immunocytes in the larva. Earlier transcription factors for pigment and blastocoelar cell development (e.g. *gcm, gata123*) have been briefly

described in the literature as appearing in the coelomic pouches,[29] but have not been investigated thoroughly.[29,39,40] The role of these factors in larvae can now be formally tested with lineage tracing during larval infection and long-term recovery. This will be an exciting and more easily accessible avenue for future work in *L. pictus*.

The data presented herein provide an initial characterization of the cellular immune components in *L. pictus*. Future work will explore how the larval immune system distinguishes between pathogenic and benign encounters in the microbially rich marine environment, and how the immune system is used during bacteria-stimulated metamorphosis. Indeed, the rapid development of this species enables direct investigation of the function of immune genes and cell types across all stages in development, especially during the construction of the rudiment and subsequent tissue remodeling during metamorphosis. In addition, the identification of which cellular components of immunity are retained between larval and post-metamorphic stages will help us understand how early life encounters may impact the adult immune system.

Our initial description of the larval *L. pictus* immune system will enable future opportunities to investigate combinatorial stressors on the protective systems of sea urchins as well. Harmful environmental agents such as xenobiotics (e.g. toxicants, "forever chemicals" and other pollutants) can impair the immune system by disrupting critical functions of immune cells (e.g. migration, signaling or cytokine release) or by impacting the differentiation of immune cell types during development.[41–44] Echinoderms have long been used for investigations on environmental stressors[45–48] (e.g. natural products from marine bacteria; anthropogenic pollutants). Sea urchin embryos are a standard toxicological model, and thus provide an ideal system for studying the influence of multiple environmental stressors (e.g. chemical exposures and bacterial infection) on the function of the immune system throughout the lifespan of this rapidly developing species.

Finally, the ability to generate stable animal lines in *L. pictus* opens the door for targeted perturbations of specific immune components through genetic manipulation. For example, CRISPR perturbation in this species has already yielded insight into immune-relevant outcomes.[48] Additional editing tools have recently been leveraged to generate stable transgenic animal lines that express fluorescent protein markers.[49] These resources can now be readily applied to questions at the intersection of immunity, development and other environmental exposures in *L. pictus*.

METHODS

Animal husbandry and larval culturing

Adult *L. pictus* were collected off the coast of Southern California and maintained in flow-through sea water tanks held at 20°C. The adults were fed fresh kelp (*Macrocystis*) *ad libitum* and the tanks were cleaned twice weekly. To collect gametes, adults were spawned by intra-coelomic injection (1-mL syringe with a 27 G needle) of 100–200 µL of 0.5 M KCl. The animals were gently shaken after injection and observed for gamete release. Females were kept submerged during spawning to minimize desiccation stress on the animal. Males were placed in a shallow dish of sea water and sperm was collected and concentrated with a glass pipette off the aboral surface of the animal and stored in an Eppendorf tube. The eggs were washed 6–10× with filtered sea water (FSW) to remove the jelly coating. The eggs were observed for quality, and estimates of density were calculated. Test fertilizations were performed to ensure high (> 98%) success fertilization. The eggs were then fertilized and set up in culture at a density no greater than 1 embryo/mL and grown with gentle agitation at 23°C. Larvae were sampled often post-fertilization to ensure that no developmental abnormalities were observed, and no immune activation occurred preceding any infection assays. Larvae were fed the red flagellated alga *Rhodamonas lens* at 2 dpf at a concentration of 3000 cells mL^{-1}. Larvae were starved overnight before infection.

Live-imaging of larval immune cell types

Live larvae at 3 dpf were imaged on either a Zeiss LSM 700 confocal microscope (Jena, Germany) with a 20× objective or a Zeiss Axio Observer.Z1 using objectives ranging from 5× to 100× oil immersion, with differential interference contrast (DIC) optics. Images were captured using the ZEN software suite with both an Axiocam 506 monochromatic camera and an Axiocam 105 color camera. Time lapses captured a full Z-stack through the entire larval body every minute for 8 min in either uninfected larvae, or larvae that had been exposed to *V. diazotrophicus* for 28 h. Measurements to micrographs were added using Fiji (National Institutes of Health, Bethesda, Maryland, USA). Composite images were rendered from Z-stacks of animals using Helicon Focus Pro Unlimited (v6.8.0, Helicon Soft Ltd). Videos for the Supplementary materials were annotated using DaVinci Resolve (v.18.6, Blackmagic Design).

Phylogenetic analysis of *L. pictus* immune gene families (macpf and IL-17)

Candidate protein sequences within the *macpf* gene family were identified within the predicted peptide sequences of *S. purpuratus* (v5.0), *L. variegatus* (v3.0) and *L. pictus* (v2.1) (Echinobase). Previously identified macpf sequences were used as queries in pblast searches against the protein sequences of each species and manually annotated to confirm identity. The

presence of a macpf domain (PF01823) was confirmed in each of the translated sequences using the web-based SMART structural motif prediction program. Protein sequences were aligned using ClustalW. Phylogenetic analysis of the resulting alignment was run in IQTree (v1.6.12) through the command line. Support values were calculated based on 1000 bootstrap replicates.

Candidate sequences for *IL-17* gene paralogs were identified within the genome sequences of *S. purpuratus* (v5.0), *L. variegatus* (v3.0) and *L. pictus* (v2.1) (Echinobase.org). Previously identified IL-17 sequences were used as tblastn queries against the three genomes and manually annotated to identify potential splice sites. The presence of an IL-17 domain (PF06083) was confirmed in each of the predicted coding sequences using HMMER. Genomic coordinates of identified paralogs are shown in Supplementary tables 5–7. A FASTA file of all the IL17 sequences used in our analysis is available upon request. Protein sequences were aligned in ClustalX2 using the Complete Alignment function. Phylogenetic analysis was performed on the IQTree Web Server using maximum likelihood methods. Support values were calculated based on 1000 bootstrap replicates.

Bacterial culture and preparation for infection assays

The marine nitrogen-fixing bacterium *V. diazotrophicus* (ATCC 33466) was cultured from frozen glycerol stocks (stored at −80°C) on marine broth media (MB2216, Difco) and grown at 15°C. To prepare bacteria for infection assay, liquid cultures grown for > 12 h were spun down (5000 × *g*) three times and washed with FSW to remove media components. Bacteria were resuspended in FSW, and a sample of the culture was diluted 1:100 or 1:1000 for counting on a Petroff-Hausser chamber to determine the cell density prior to use for infections.

Larval infection assays

Larvae were infected with *V. diazotrophicus* at a density of 1×10^7 cells mL^{-1}, as described in Ho *et al.* (2016).[8] Briefly, prepped bacteria were added to cultures of larvae for a simple sea water exposure and left in culture for up to 24-h post-exposure (hpe) for larvae to interact with and feed on the bacteria. Larvae were sampled at 0, 6, 12 and 24 hpe and imaged live on a Zeiss LSM 700 confocal microscope (Jena, Germany) with a 20× objective using differential interference contrast (DIC). The number of migratory pigment cells in each individual larva was counted by eye during live imaging. Measurements were added using ImageJ (National Institutes of Health, Bethesda, MD, USA).

Larval fixation for hybridization-chain reaction (HCR) imaging

Whole larvae were collected from the *Vibrio-infected* cultures (prepared as above) immediately prior to exposure to *V. diazotrophicus* (hour 0), and at 2, 6, 12 and 24 hpe. Control samples were collected from uninfected cultures at identical timepoints. To concentrate the larval samples, an aliquot of each culture was slowly passed over a 70-µm mesh filter. Larvae were transferred into 1.5-mL Eppendorf tubes, allowed to settle on ice, and rinsed once with 1 mL FSW. The larvae were then incubated in 500 µL FSW with 50 µL 4.45 M NaCl for 5 min to remove cilia. The sample was then rinsed again with 1 mL FSW, and then added to a 2-mL cryogenic tube containing 500 µL fixation buffer and 500 µL 16% PFA (f.c. 4% PFA). The samples were placed on a nutator for gentle agitation at 4°C for 24 h. After the 24-h fixation period, each tube was transferred onto ice and 100 µL 1 M glycine (made with 1 mM EDTA in calcium–magnesium-free sea water [CMFSW]) was added. After the larvae settled to the bottom of the tube (~5 min), the sample was rinsed 2× 10 min with 1 mL of 1× PBST and 100 µL 1 M glycine, followed by 1× 10 min rinse with 1× PBST. Larvae were rinsed 3× 10 min into 70% EtOH. Samples were stored at −20°C in 70% EtOH until use in the HCR protocols described below.

In situ hybridization chain reaction (HCR)

Probes were selected from a probe library containing HCR probe sets designed for all predicted coding sequences for *L. pictus*. Probe sets were designed using a custom wrapper script to automate insitu_probe_generator (https://github.com/rwnull/insitu_probe_generator/tree/v0.3.2) for the design of all probe-hairpin combinations for all coding sequences. Probes were purchased from Integrated DNA Technologies (IDT; Coralville, IA, USA), and amplification hairpins were purchased from Molecular Instruments (El Monte, CA, USA). Probe sequences are listed in Supplementary table 1.

HCR processing steps were adapted from the molecular instruments HCR™ RNA-FISH protocol for whole-mount sea urchin embryos (*S. purpuratus*), optimized for *L. pictus* larvae ≥ 72 hpf.[20,27] Approximately 100 larvae from each fixed sample were rehydrated gradually from 70% into 200 µL of 5× SSCT through 3× 10 min washes. 5× SSCT was then aspirated and 50 µL of probe hybridization buffer (Molecular Instruments) was added and the samples were pre-hybridized at 37°C for 30 min. Probe solution was prepared with 1.5 µL of 1 µM stock probe set to 50 µL of probe hybridization buffer at 37°C. Probe solution was added to the samples and gently mixed to reach a final hybridization volume of 100 µL. Samples were incubated for 24 h at 37°C. After incubation, 150 µL of preheated probe wash buffer (Molecular Instruments) was added to each tube of larvae and incubated at 37°C for 5 min. Excess probes were removed by washing the samples with 200 µL of probe wash buffer at 37°C 2× 10 min, then 2× 30 min. The samples were then rinsed into 5× SSCT with 2× 10 min washes. Hairpin solutions were prepared by snap cooling 6 pmol of each hairpin (h1 and h2) per sample in separate tubes by heating at 95°C for 90 s and cooling back to room temperature in a dark drawer for 30 min. Hairpins were added to room temperature amplification buffer (Molecular Instruments) at a ratio of 6 pmol:50 µL of the amplification buffer. 5× SSCT was removed from the samples and the 50 µL of hairpin solution

was added and incubated in the dark for 24 h at room temperature. After hairpin incubation, 150 µL of 5× SSCT was added to the sample and then incubated for 5 min at room temperature. Excess hairpins were removed by washing with 200 µL of 5× SSCT at room temperature for 3× 10 min, then 2× 30 min. DAPI nuclear stain (Invitrogen, Waltham, MA) was added to the second 30 min wash at a final concentration of 300 µM DAPI in 5× SSCT. Samples were rinsed once more in 5× SSCT and stored in 5× SSCT at 4°C protected from light before confocal imaging.

Confocal imaging of HCR in sea urchin larvae

Prior to imaging, larva samples were transferred into 80% glycerol using a stepwise rinse of 70/30 5× SSCT:100% glycerol, 50/50 and 20/80. Larvae were gently plated into wells of a Cellvis glass bottom 384-well plate (Mountain View, California, USA) at a density of ~20 larvae per well. Confocal microscopy was performed on a Molecular Devices ImageXpress HT.ai (San Jose, California, USA) using a 20× Nikon Plan Apochromatic objective. Laser channels used in this study include 750, 647, 594 and 405 nm, along with corresponding emission filters. All samples were imaged in 3 µm Z-stacks with a 100 ms exposure time and 50% laser power. Image processing was conducted using FIJI (ImageJ), including 2D maximum projections of the appropriate range of stacks, scale bar generation (pixel ratio of 3.416 pixels/1 µm), and cropping of single larvae from a field of view. Embryos that were processed without probes served as a negative control to assess non-specific signal deriving from reagent chemistry and the addition of metastable fluorescent hairpins (Supplementary figure 3).

Data quantifying phenotype distributions were scored from Z-stacks of 25 larvae each from three mate pairs ($n = 75$ total). Briefly, each Z-stack was analyzed, and phenotypes were binned according to the expression patterns for each target gene. For *srcr142*, expression in the coelomic pouch territory is a novel finding from this study and thus our scoring details this phenotype distribution specifically. Counts from scoring fluorescence Z-stacks of the larvae (Supplementary tables 3 and 4) were visualized using GraphPad Prism 9 (v.9.s.0.332) and presented as stacked bars for the percentages of larvae scored.

Quantitative fluorescence intensity data of larval images from hybridization chain reaction experiments was measured using FIJI (ImageJ). Z-stacks were imaged throughout the entire larvae and subsequently used for measurements. The slices from each Z-stack were compressed into a maximum intensity projection. The mean fluorescence of a set circle area of 4421 pixels (which fully encapsulates the coelomic pouch territory) was measured at each of four target anatomical regions (e.g. coelomic pouch, oral hood or gut) per larva. Additionally, the mean fluorescence intensity of a background region of equal size and immediately adjacent to the target region was measured for each anatomical region in each larva for downstream calculations and statistical analyses. Quantitative fluorescence data were collected from five individual larvae each from three mate pairs ($n = 15$ total). Three-dimensional rendering of confocal images of larvae were generated using Imaris 10.1 (Oxford Instruments, Abingdon, UK).

Statistical analyses

Data quantifying the migratory pigment cell response in *L. pictus* larvae (Figure 3a) were analyzed and visualized using the GraphPad Prism 9 (v.9.s.0.332) software package. Each individual experiment was performed with a single mate pair (sibling larvae) and treatment significance was determined using minimum $n = 3$ batches (mate pairs) of sibling larvae. Treatment significance was determined using ANOVA. Data were plotted using the GraphPad suite and exported as high quality (300 dpi) image files and additional labeling was added in Adobe Illustrator.

Data quantifying the fluorescent signal in the larvae hybridization chain reaction experiments were analyzed and visualized using GraphPad Prism 9 (v.9.s.0.332) software package. Net fluorescence was calculated as the mean fluorescence intensity minus the intensity of the background signal. A two-way ANOVA with multiple comparisons (Tukey test) was performed in GraphPad Prism to determine statistical significance of the data. Data were plotted using the GraphPad suite and exported as high quality (300 dpi) image files and additional labeling was added in Adobe Illustrator.

ACKNOWLEDGMENTS

The authors thank two anonymous reviewers for helpful critique and improvements to the manuscript. We thank Dr Nicholas J Shikuma for use of the Zeiss Axio Observer for live imaging of sea urchin larval immunocytes. The authors also thank members of the Schrankel and Hamdoun labs for assistance with the experimental set up, animal husbandry and culture handling. CSS thanks San Diego State University for generous start-up support enabling this work. This work was also supported by NIH ES027921 to AH.

AUTHOR CONTRIBUTIONS

Katherine T Nesbit: Conceptualization; data curation; formal analysis; investigation; methodology; project administration; supervision; validation; visualization; writing – original draft; writing – review and editing. **Alexis Cody Hargadon:** Data curation; formal analysis; writing – review and editing. **Gloria D Renaudin:** Data curation; formal analysis; writing – review and editing. **Nicholas D Kraieski:** Formal analysis; writing – review and editing. **Katherine M Buckley:** Investigation; writing – review and editing. **Emily Darin:** Methodology. **Yoon Lee:** Methodology. **Amro Hamdoun:** Conceptualization; resources; supervision; writing – review and editing. **Catherine S Schrankel:** Conceptualization; data curation; formal analysis; funding acquisition; resources; supervision; writing – review and editing.

CONFLICT OF INTEREST

The authors declare no conflicts of interest.

DATA AVAILABILITY STATEMENT

The data that support the findings of this study are available in the supplementary material of this article. A FASTA file of all the IL17 sequences used in our analysis is available upon request. Any additional data not contained within the supplementary materials (e.g. full genomic data for sea urchin species) are available through publicly accessible databases (Echinobase: https://www.echinobase.org/echinobase/ and NCBI: BioProject PRJNA647794).

REFERENCES

1. Groër M, Meagher MW, Kendall-Tackett K. An overview of stress and immunity. In: Kendall-Tackett K, ed. The Psychoneuroimmunology of Chronic Disease: Exploring the Links between Inflammation, Stress, and Illness. Washington, DC: American Psychological Association; 2010:9–22.
2. Pinsino A, Matranga V. Sea urchin immune cells as sentinels of environmental stress. *Dev Comp Immunol* 2015; **49**: 198–205.
3. Metchnikoff E. Untersuchungen uber die intracellulare Verdauung bei wirbellosen Thieren. *Arb Zoo Ins Univ wien u Zoo Sta Triest* 1884; **5**: 141.
4. Furukawa R, Takahashi Y, Nakajima Y, Dan-Sohkawa M, Kaneko H. Defense system by mesenchyme cells in bipinnaria larvae of the starfish, *Asterina pectinifera*. *Dev Comp Immunol* 2009; **33**: 205–215.
5. Silva JR. The onset of phagocytosis and identity in the embryo of *Lytechinus variegatus*. *Dev Comp Immunol* 2000; **24**: 733–739.
6. Rast JP, Smith LC, Loza-Coll M, Hibino T, Litman GW. Genomic insights into the immune system of the sea urchin. *Science* 2006; **314**: 952–956.
7. Buckley KM, Ho ECH, Hibino T, *et al.* IL17 factors are early regulators in the gut epithelium during inflammatory response to *Vibrio* in the sea urchin larva. *elife* 2017; **6**: e23481.
8. Ho EC, Buckley KM, Schrankel CS, *et al.* Perturbation of gut bacteria induces a coordinated cellular immune response in the purple sea urchin larva. *Immunol Cell Biol* 2016; **94**: 861–874.
9. Pancer Z, Rast JP, Davidson EH. Origins of immunity: transcription factors and homologues of effector genes of the vertebrate immune system expressed in sea urchin coelomocytes. *Immunogenetics* 1999; **49**: 773–786.
10. Smith LC, Rast JP, Brockton V, *et al.* The sea urchin immune system. *Invert Surv J* 2006; **3**: 25–39.
11. Calestani C, Rast JP, Davidson EH. Isolation of pigment cell specific genes in the sea urchin embryo by differential macroarray screening. *Development* 2003; **130**: 4587–4596.
12. Smith VJ, Desbois AP, Dyrynda EA. Conventional and unconventional antimicrobials from fish, marine invertebrates and micro-algae. *Mar Drugs* 2010; **8**: 1213–1262.
13. Gibson AW, Burke RD. The origin of pigment cells in embryos of the sea urchin *Strongylocentrotus purpuratus*. *Dev Biol* 1985; **107**: 414–419.
14. Tamboline CR, Burke RD. Secondary mesenchyme of the sea urchin embryo: ontogeny of blastocoelar cells. *J Exp Zool* 1992; **262**: 51–60.
15. Hibino T, Loza-Coll M, Messier C, *et al.* The immune gene repertoire encoded in the purple sea urchin genome. *Dev Biol* 2006; **300**: 349–365.
16. Nesbit KT, Fleming T, Batzel G, *et al.* The painted sea urchin, *Lytechinus pictus*, as a genetically-enabled developmental model. *Methods Cell Biol* 2019; **150**: 105–123.
17. Nesbit KT, Hamdoun A. Embryo, larval, and juvenile staging of *Lytechinus pictus* from fertilization through sexual maturation. *Dev Dynam* 2020; **249**: 1334–1346.
18. Warner JF, Lord JW, Schreiter SA, Nesbit KT, Hamdoun A, Lyons DC. Chromosomal-level genome assembly of the painted sea urchin *Lytechinus pictus*, a genetically enabled model system for cell biology and embryonic development. *Genome Biol Evol* 2021; **13**: evab061.
19. Choi HM, Chang JY, Trinh LA, Padilla JE, Fraser SE, Pierce NA. Programmable in situ amplification for multiplexed imaging of mRNA expression. *Nate Biotech* 2010; **28**: 1208–1212.
20. Choi HM, Schwarzkopf M, Fornace ME, *et al.* Third-generation *in situ* hybridization chain reaction: multiplexed, quantitative, sensitive, versatile, robust. *Development* 2018; **145**: dev165753.
21. Bi S, Yue S, Zhang S. Hybridization chain reaction: a versatile molecular tool for biosensing, bioimaging, and biomedicine. *Chem Soc Rev* 2017; **46**: 4281–4298.
22. Buckley KM, Rast JP. Immune activity at the gut epithelium in the larval sea urchin. *Cell Tissue Res* 2019; **377**: 469–474.
23. Paganos P, Ronchi P, Carl J, *et al.* Integrating single cell transcriptomics and volume electron microscopy confirms the presence of pancreatic acinar-like cells in sea urchins. *Front Cell Dev Biol* 2022; **10**: 991664.
24. Perillo M, Wang YJ, Leach SD, Arnone MI. A pancreatic exocrine-like cell regulatory circuit operating in the upper stomach of the sea urchin *Strongylocentrotus purpuratus* larva. *BMC Evol Biol* 2016; **16**: 1–15.
25. Holland ND, Lauritis JA. The fine structure of the gastric exocrine cells of the purple sea urchin, *Strongylocentrotus purpuratus*. *Trans Am Micro Soc* 1968; **87**: 201–209.
26. Guerinot M, West P, Lee J, Colwell R. *Vibrio diazotrophicus* sp. nov., a marine nitrogen-fixing bacterium. *Int J Syst Evol Microbiol* 1982; **32**: 350–357.
27. Lee Y, Tjeerdema E, Kling S, Chang N, Hamdoun A. Solute carrier (SLC) expression reveals skeletogenic cell diversity. *Dev Biol* 2023; **503**: 68–82.
28. Pancer Z. Dynamic expression of multiple scavenger receptor cysteine-rich genes in coelomocytes of the purple sea urchin. *Proc Natl Acad Sci USA* 2000; **97**: 13156–13161.

29. Schrankel C. Gene Regulatory Control of Immune Cell Specification and Differentiation in the Sea Urchin Embryo and Larva. 2017. University of Toronto (Canada). https://tspace.library.utoronto.ca/handle/1807/80634.
30. Buchmann K. Evolution of innate immunity: clues from invertebrates via fish to mammals. *Front Immunol* 2014; **5**: 459.
31. Flajnik MF, Kasahara M. Origin and evolution of the adaptive immune system: genetic events and selective pressures. *Nat Rev Genet* 2010; **11**: 47–59.
32. Wray GA. The evolution of larval morphology during the post-Paleozoic radiation of echinoids. *Paleobiology* 1992; **18**: 258–287.
33. Wray GA, Lowe CJ. Developmental regulatory genes and echinoderm evolution. *Syst Biol* 2000; **49**: 28–51.
34. Gonzalez P, Lessios HA. Evolution of sea urchin retroviral-like (SURL) elements: evidence from 40 echinoid species. *Mol Biol Evol* 1999; **16**: 938–952.
35. Sobinoff AP, Dando SJ, Redgrove KA, *et al*. *Chlamydia muridarum* infection-induced destruction of male germ cells and sertoli cells is partially prevented by *chlamydia major* outer membrane protein-specific immune CD4 cells. *Biol Reprod* 2015; **92**: 1–13.
36. Pelzer ES, Allan JA, Cunningham K, *et al*. Microbial colonization of follicular fluid: alterations in cytokine expression and adverse assisted reproduction technology outcomes. *Hum Reprod* 2011; **26**: 1799–1812.
37. Borges ED, Berteli TS, Reis TF, Silva AS, Vireque AA. Microbial contamination in assisted reproductive technology: source, prevalence, and cost. *J Asst Reprod Gen* 2020; **37**: 53–61.
38. Ermolaeva MA, Segref A, Dakhovnik A, *et al*. DNA damage in germ cells induces an innate immune response that triggers systemic stress resistance. *Nature* 2013; **501**: 416–420.
39. Solek CM, Oliveri P, Loza-Coll M, *et al*. An ancient role for Gata-1/2/3 and Scl transcription factor homologs in the development of immunocytes. *Dev Biol* 2013; **382**: 280–292.
40. Ransick A, Rast JP, Minokawa T, Calestani C, Davidson EH. New early zygotic regulators expressed in endomesoderm of sea urchin embryos discovered by differential array hybridization. *Dev Biol* 2002; **246**: 132–147.
41. Leijs MM, Koppe JG, Olie K, van Aalderen WM, de Voogt P, ten Tusscher GW. Effects of dioxins, PCBs, and PBDEs on immunology and hematology in adolescents. *Environ Sci Technol* 2009; **43**: 7946–7951.
42. Liu X, Zhan H, Zeng X, Zhang C, Chen D. The PBDE-209 exposure during pregnancy and lactation impairs immune function in rats. *Mediators Inflamm* 2012; **2012**: 692467.
43. Watanabe W, Shimizu T, Hino A, Kurokawa M. Effects of decabrominated diphenyl ether (DBDE) on developmental immunotoxicity in offspring mice. *Environ Toxicol Pharmacol* 2008; **26**: 315–319.
44. Forawi HA, Tchounwou PB, McMurray RW. Xenoestrogen modulation of the immune system: effects of dichlorodiphenyltrichloroethane (DDT) and 2, 3, 7, 8-tetrachlorodibenzo-p-dioxin (TCDD). *Rev Environ Health* 2004; **19**: 1–14.
45. Hamdoun AM, Griffin FJ, Cherr GN. Tolerance to biodegraded crude oil in marine invertebrate embryos and larvae is associated with expression of a multixenobiotic resistance transporter. *Aq Tox* 2002; **61**: 127–140.
46. Goldstone J, Hamdoun A, Cole B, *et al*. The chemical defensome: environmental sensing and response genes in the *Strongylocentrotus purpuratus* genome. *Dev Biol* 2006; **300**: 366–384.
47. Gökirmak T, Campanale JP, Shipp LE, Moy GW, Tao H, Hamdoun A. Localization and substrate selectivity of sea urchin multidrug (MDR) efflux transporters. *J Biol Chem* 2012; **287**: 43876–43883.
48. Vyas H, Schrankel CS, Espinoza JA, *et al*. Generation of a homozygous mutant drug transporter (ABCB1) knockout line in the sea urchin *Lytechinus pictus*. *Development* 2022; **149**: dev200644.
49. Jackson EW, Romero E, Lee Y, Kling S, Tjeerdema E, Hamdoun A. Stable germline transgenesis using the Minos Tc1/mariner element in the sea urchin, *Lytechinus pictus*. *Development* 2024; **151**: dev202991.

SUPPORTING INFORMATION

Additional supporting information may be found online in the Supporting Information section at the end of the article.